

Analysis of the Effects of Path Properties on Autonomous Motion Control of a Hydraulic Tracked Vehicle

Teemu Mononen

Laboratory of Automation and Hydraulic
Engineering
Tampere University of Technology
Tampere, Finland
teemu.mononen@tut.fi

Mohammad M. Aref

Laboratory of Automation and Hydraulic
Engineering
Tampere University of Technology
Tampere, Finland
m.aref@ieee.org

Jouni Mattila

Laboratory of Automation and Hydraulic
Engineering
Tampere University of Technology
Tampere, Finland
jouni.mattila@tut.fi

Abstract—Mobile working machines have recently been developed towards field robotics systems that are more self-aware, intelligent, autonomous and energy-efficient. Such autonomy can offer advantages in, for example, construction sites, where a number of tasks involve accurate path following. From the robotic viewpoint, a mobile robot is supposed to follow the desired values perfectly to remain on a certain path as long as its localization provides the necessary pose feedback. In field robotics, especially in the cases of hydraulic working machines, there are nonlinear system dynamics affecting the mobile platform, which makes accurate motion control challenging. The sources of these nonlinearities can be the internal system dynamics or environmental effects. Due to the use of generic autonomous motion planning and control methods in the existing literature, there are certain effects of hydrostatic driveline on the system that have been overlooked. To fill such a gap, this paper first analyzes and points out the effects of geometrical path properties on the performance of hydraulic actuators in path-following control. Then, using a closed-loop model of a skid-steered vehicle with hydraulic propulsion, we show simulation results with the machine following paths with different curvatures around an obstacle. Analysis of the results show the significant role of the system dynamics in shifting the optimal path when the dynamics of the driveline and terrain contact are included.

Keywords—mobile robot, path-following control, hydrostatic transmission

I. INTRODUCTION

Autonomous vehicles have been researched in a vast amount of studies in recent years. In construction site applications, vehicle autonomy can introduce more effective workflows and high-level organization of tasks among autonomous machines. Nowadays, numerous heavy construction vehicles rely on hydrostatic transmission (HST) systems and tracks to provide propulsion. To control heavy-duty vehicle locomotion as intricately and safely as light weight wheeled robots requires adjustments in the control design process at both high and low level. An important factor is the dynamic behavior of the HST, which will affect the path following performance and optimum

path generation. Tight curves will most likely cause tracking error and returning to the desired path after such a turn causes oscillation [1]. Path following design mainly consists of path planning, path following control and vehicle localization. In this paper, we consider path following control, but point out the effects of our findings on path planning.

In the previous mobile robot path following studies, vehicle dynamics govern the design. In a number of these studies, the actuator dynamics are not taken into account (e.g. [2], [3]) or are simplified into bounded actuation [4] [5]. In hydraulic mobile robots, these dynamics affect the vehicle behavior and path following controller performance. For instance, in [1], the authors propose path-following control for a hydraulically actuated articulated-frame-steering (AFS) machine, noticing that the delays posed by real hydraulic circuit dynamics cause oscillatory behavior in the achieved path. In many studies, the actuator dynamics are considered in actuator level control (e.g. [6]). From the path planning point of view, it is beneficial to consider actuator dynamics to generate paths allowing, e.g., low power consumption or limited torque [7]. The knowledge of the effects of path geometry can be useful in achieving this. However dynamic limitations have been overlooked for skid-steering mechanisms due to their capabilities in driving on high-curvature path.

In this paper, we highlight the effects of the desired path properties on the hydro-mechanical losses and power requirements of a skid-steered tracked mobile platform with a HST. After considering the properties of the path in an analytical study, the effects of path curvature κ are found to cause most of the losses in the hydraulic circuit. Furthermore, we present simulation results of path-following scenarios using a vehicle model also including the vehicle body dynamics and terrain interactions. We conclude that the shortest path around an obstacle is suboptimal considering power consumption. Instead, a compromise between a short and long path is found to be more desirable from this point of view. We project these results useful in the future path following research for mobile platforms with hydraulic propulsion.

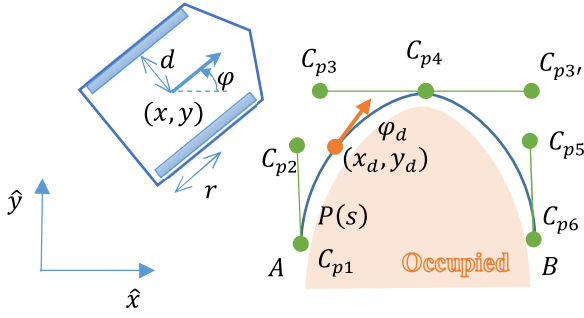


Fig. 1. The skid-steering platform and formulation of desired path values as control points.

This paper is organized as follows: in section II, the vehicle model is presented along with vehicle and hydraulic dynamics. In section III, the path parameterization and path-following control strategy are introduced. Section IV includes analysis of the dependencies between hydro-mechanical losses and the path properties along with simulation results of path following with different path curvatures. Section V concludes the present study.

II. VEHICLE MODEL

A. Kinematics

In skid steering, the heading angle of the vehicle is controlled by manipulating the rotational velocities of track driving wheels on each side of the vehicle. To turn right, for example, the left track must have larger velocity compared to the right track. This is accomplished by rotating the corresponding track driving wheels at desired speeds. The kinematic model of the skid steered machine relates the Cartesian velocities and heading to the rotation speeds of the vehicle track wheels. The principle of skid-steering is presented in Fig. 1. The inverse kinematics are attained using equations (1) and (2):

$$u_l = \frac{v - \omega d}{r} \quad (1)$$

$$u_r = \frac{v + \omega d}{r}, \quad (2)$$

where u_l and u_r are the left and right track rotation speeds, respectively, v is the velocity of the vehicle and ω is the time derivative of the heading angle φ .

B. Dynamics

In addition to mass and inertia of the vehicle itself, the dynamic model composes of track-terrain interactions and rolling resistance. The vehicle model can be presented in a simplified way using equation (3).

$$m\ddot{x} = \Sigma F_F - \Sigma F_R \quad (3)$$

where ΣF_F contains the driving forces and ΣF_R the resisting forces. A detailed description of the dynamics is omitted to save space. In this study, the mass of the vehicle was selected as 13,500 kg. The vehicle was modeled using MATLAB Simulink and Simscape Multibody Contact Forces Library [8]. Forces affecting the undercarriage are illustrated in Fig. 2 and Fig. 3.

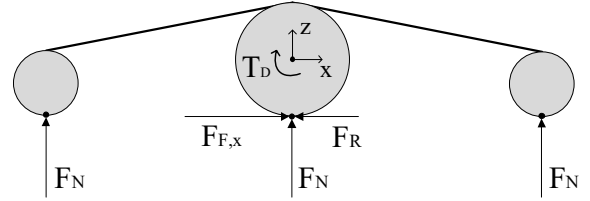


Fig. 2. Side view of the forces affecting the track through three track wheels (grey). T_D represents the driving torque, F_F the friction force and F_R the resisting force.

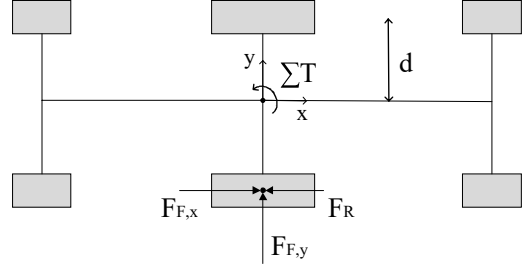


Fig. 3. Top view of the forces and torques affecting the undercarriage. To save space, only the forces affecting one of the two sides are illustrated.

The vehicle is modeled such that driving torques are inserted to the middle wheels, which allows the vehicle to turn in place. The friction forces affecting the track are described in equations (4) and (5) as in [8].

$$F_f = \mu F_n \quad (4)$$

$$\mu = \begin{cases} \frac{v_{poc}\mu_s}{v_{th}}, & v_{poc} < v_{th} \\ \mu_s - v_{poc} \frac{\mu_s - \mu_k}{0.5v_{th}}, & v_{th} \leq v_{poc} \leq 1.5v_{th} \\ \mu_k, & v_{poc} > v_{th}, \end{cases} \quad (5)$$

Where F_n is the normal force affecting the wheel, μ_s and μ_k are static and kinetic friction coefficients, v_{poc} is the velocity of the point of contact and v_{th} the threshold velocity at the point of contact. Contact force at the track wheel position is presented in equation (6) to soften the hard contact using a spring-damper model [8].

$$F_z = \begin{cases} kz_c + bv_c, & z_c > 0, v_c > 0 \\ kz_c, & z_c > 0, v_c < 0 \\ 0, & z_c \leq 0, \end{cases} \quad (6)$$

where k represents stiffness, b damping, z_c the contact position and v_c the contact velocity.

C. Hydraulics

In the tracked vehicle of this study, the propulsion system includes a dual path HST, in which a separate pump and motor is installed for each track. The fixed displacement motor rotation speed is controlled by manipulating the pump swashplate angle, as illustrated in Fig. 4. For simplicity, the auxiliary valves and pumps are denoted as grey boxes between the pressure lines. The pressure level is kept between 25 and 450 bars.

The simulation model of the hydraulic circuit includes two identical circuits each containing a variable displacement pump

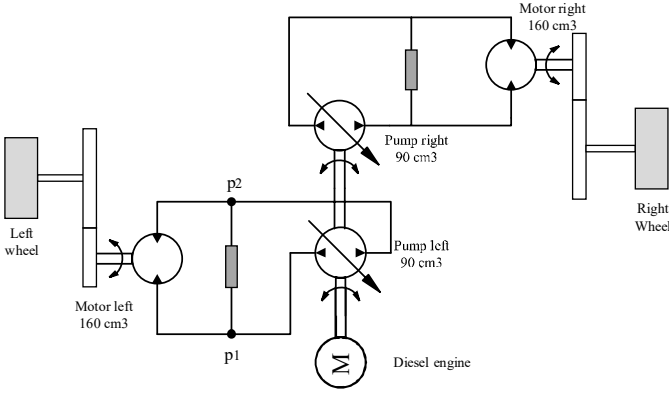


Fig. 4. A simplified hydraulic diagram of the dual path HST.

and a fixed displacement motor. Both pumps are driven at a constant rotation velocity by a single diesel engine, as illustrated in Fig. 4. The torque produced by the hydraulic motors is transferred to the track wheels using a gear. The flow and torque equations for the pumps and motors (subscripts p and m , respectively) are presented in equations (7)-(10) [9] [10].

$$Q_p = \epsilon_p n_p V_p - C_{i,p} \Delta p \quad (7)$$

$$T_p = \frac{V_p \Delta p}{2\pi} (\epsilon_p + C_{f,p}) + C_{d,p} \mu V_p n_p \quad (8)$$

$$Q_m = n_m V_m + C_{i,m} \Delta p \quad (9)$$

$$T_m = \frac{V_m \Delta p}{2\pi} (1 - C_{f,m}) - C_{d,m} \mu V_m n_m \quad (10)$$

where ϵ_p is the pump swashplate angle ($\in [-1, 1]$), n the rotation speed, V the maximum displacement, C_i internal leakage coefficient, C_f coulomb friction coefficient, C_d viscous friction coefficient and Δp the pressure difference between the inlet and outlet ports of the component. The pressure dynamics in the hose between a pump and motor can be expressed as:

$$\dot{p} = \frac{B_{eff}}{V} (Q_{in} - Q_{out}), \quad (11)$$

where Q_{in} is the oil volume entering the hose and Q_{out} the volume leaving it. B_{eff} is the effective bulk modulus and V the hose volume.

D. HST Control and Model Verification

The control of wheel rotation speed is realized using PI-controllers with the pump swashplate angles as the control variables. In path following control, a high-level controller produces velocity setpoints for these low-level controllers that then produce control signals to manipulate the pump swashplate angle accordingly. The PI-controllers have fixed gains that were tuned so that high-frequency oscillations in e.g. fluid pressure do not occur due to high controller gains, but reference tracking is satisfactory. The control scheme of the motor rotation speed is simple as it is calculated only by the pump displacement after consideration of losses.

To verify the vehicle model, open loop tests were conducted and the system states were recorded. The vehicle was expected

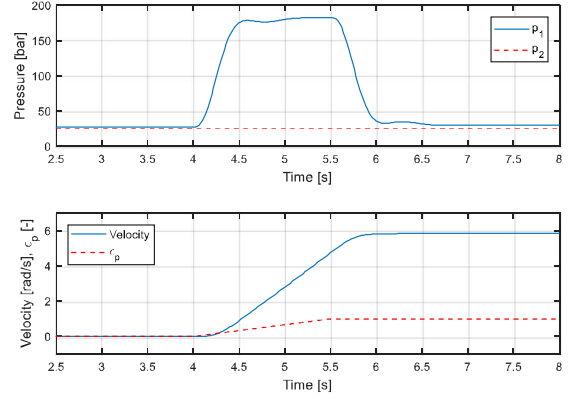


Fig. 5. The open-loop response of the system to pump swashplate opening from 0 to 1. Pressure in ports 1 and 2 (Fig. 4) and wheel rotation velocity.

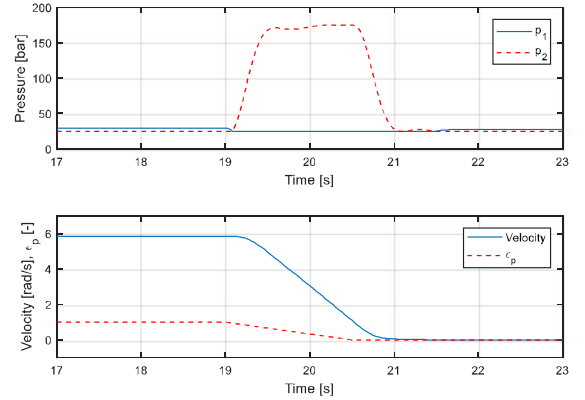


Fig. 6. The open-loop response of the system to pump swashplate closing from 1 to 0. Pressure in ports 1 and 2 (Fig. 4) and wheel rotation velocity.

to behave quite similarly as the skid steered mobile machine described in [10]. The open loop tests were conducted as in [10], by opening and closing the pump swashplates. Similar variables are plotted in Fig. 5 and Fig. 6 to make a comparison to [10]. In Fig. 5 and Fig. 6 it is evident, that the responses of our model are very similar to the ones presented in [10], but with more damping. Based on this, the system model behavior is satisfactory.

III. PATH FOLLOWING CONTROL

A. Path Parameterization

The main task of the field robot is the sequential following of several pieces of a path, which is referred to as $P(s)$. This path is usually created based on control points with polynomial interpolations, such as in Bézier curves with control points shown in Fig. 1. The path parameter, s determines the location of the desired pose on the path, which is normalized by the path length such that $P(0)$ stands for the beginning of the path and $P(1)$ for the end of the path at each piece to cover desired values as:

$$P(s) = \begin{bmatrix} x_d(s) \\ y_d(s) \end{bmatrix} \quad (12)$$

This formulation leads into a description of kinematic variables in terms of geometrical properties and motion

primitives. In addition to control purposes, we will use it in section IV to determine the effects of path properties on the hydraulic circuit performance. In this notation, velocities are calculated obeying the chain rule:

$$v_d(t) = \frac{\partial s}{\partial t} \frac{\partial}{\partial s} P(s), \quad (13)$$

that can be rewritten in a shorter form as $v_d = \dot{s} P'$ or $v_d = \dot{s} v_s$, where v_s is rate of displacement on the path with respect to changes in the path parameter s . This formulation is borrowed from the path-follower control methods, such as in [4]. The method is applicable to the angular velocity of the robot obeying the unicycle model and its desired heading should be tangent to path, as it determines direction of the velocity vector too.

$$\omega_d(t) = \dot{s} \kappa(s) v_s(s), \quad (14)$$

where $\kappa(s)$ is the curvature of $P(s)$. Moreover, based on the path definition, the distribution of desired velocities for each side of the skid-steered robot depend on different parameters, such as motion speed, vehicle architecture and path geometry. To highlight this relationship, we reorganize simplified kinematic equations:

$$\begin{bmatrix} u_{dl} \\ u_{dr} \end{bmatrix} = \underbrace{\dot{s}(t) v_s(s)}_{\text{motion speed}} \underbrace{\begin{bmatrix} 1/r & -d/r \\ 1/r & d/r \end{bmatrix}}_{\text{vehicle structure}} \underbrace{\begin{bmatrix} 1 \\ \kappa_s(s) \end{bmatrix}}_{\text{path geometry}} \quad (15)$$

Regardless of actuator dynamics, control methods, and vehicle architecture, this equation highlights a conceptual design point. Independent of time and time derivatives, the path geometry can significantly affect distribution of motion among the vehicle tracks. In section IV, we show that this relationship can play a significant role in the performance and power consumption of a hydraulic autonomous vehicle. In this paper, modeling is done to analyze autonomous functionalities of the robot. To this end, we present a modified formulation of the motion parameters to consider path parameter in the kinematic equations of motion. This way, we can analyze the effects of variations in the vehicle's behavior caused by (a) the path shape, (b) internal dynamics, (c) ground contact, and their interaction with each other. For this separation, the model for feedback data is calculated in time domain while the feedback terms are formulated to distinguish between the path parameters and vehicle model.

B. Path-following Control

To pursue the path $P(s)$, we use a path-following control scheme, where control error is defined as:

$$\begin{bmatrix} \varphi_e \\ x_e \\ y_e \end{bmatrix} = \begin{bmatrix} 1 & 0 & 0 \\ 0 & \cos\varphi_d & \sin\varphi_d \\ 0 & -\sin\varphi_d & \cos\varphi_d \end{bmatrix} \begin{bmatrix} \varphi - \varphi_d \\ x - x_d \\ y - y_d \end{bmatrix} \quad (16)$$

The control law to reject this error is proven in [11] to be:

$$\begin{bmatrix} v \\ \omega \end{bmatrix} = \begin{bmatrix} (v_d - k_1 |v_d| (x_e + y_e \tan \varphi_e)) \sec \varphi_e \\ \omega_d - (k_2 v_d y_e + k_3 |v_d| \tan \varphi_e) \cos^2 \varphi_e \end{bmatrix} \quad (17)$$

Therefore, the control effort for the left and right track becomes:

$$\begin{bmatrix} u_l \\ u_r \end{bmatrix} = \dot{s} \begin{bmatrix} u_{pos} - v_s d u_{rot} \\ u_{pos} + v_s u_{rot} \end{bmatrix}, \quad (18)$$

where translational and rotational parts are calculated as:

$$\begin{aligned} u_{pos} &= v_s - k_1 |v_s| (x_e + y_e \tan \varphi_e) \sec \varphi_e \\ u_{rot} &= d \kappa - d (k_2 y_e \\ &\quad + k_3 \text{sign}(v_s) \tan \varphi_e) \cos^2 \varphi_e \end{aligned} \quad (19)$$

Now, we can use u_l and u_r as the path-following inputs for the hydraulic actuator controllers that drive the tracks by supplying the necessary pressure and flow into the hydraulic motors on the left and right side. Therefore, the elements of (19) have direct effect on the resultant values of hydraulic and mechanical loss addressed in equations (7)-(10).

IV. RESULTS AND DISCUSSION

A. Analysis of losses

As stated above, the hydraulic actuators are prone to variable energy loss mainly depending on pressure differences and flow rates. Due to numerous affecting factors, and use of cascade controllers to implement path following, we illustrate the effects of selected elements of (18) and (19) on the robot's total loss.

First, we analyze the changes of the desired values and their effect on the equivalent torque loss. As illustrated in Fig. 7, the desired speed $\dot{s} v_s$ and path curvature can affect maintaining pressure and torque loss because of increasing effects of friction and leakage. As expected, higher velocities can increase the T_{loss} near linearly. The effect of $\kappa(s)$ is important in this analysis. As shown in the figure, higher path curvatures can change the behavior of the system by changing the linear rate of changes caused by the other factors. Thus, increasing the magnitude of $\kappa(s)$ for values higher than 1 demand more work from the motors, pumps and therefore from the diesel engine. Based on this coupling, we can expect lower performance and higher power consumption on tighter turns of the robot. Note that $\kappa(s)$ only depends on the path geometry and it is known in the path planning phase. Therefore, it is possible to consider these properties of hydraulic field robots to determine their configuration space or plan their route.

Once higher values of $\kappa(s)$ are given the system becomes subject of demands for faster changes in many dynamical properties. To demonstrate this effect, we also consider the torque loss based on the control equations assumed to be functions of only the heading error φ_e and the desired velocity $\dot{s} v_s$. As shown in Fig. 8, although higher velocities can cause larger torques, in case of higher curvatures, any other change faces sharper slope. For instance, errors of heading can cause larger changes of the power demand in sharper turns. These points are also verified by analysis of power, and performance in autonomous driving on a set of paths with different curvatures, as discussed in the next section.

B. Simulation results

In the test scenario, we generated five paths from point A to point B around an obstacle, whose corner was situated at (25, 35) in the world coordinate frame. For all paths, the start and end poses were identical, but the turning radius past the obstacle was

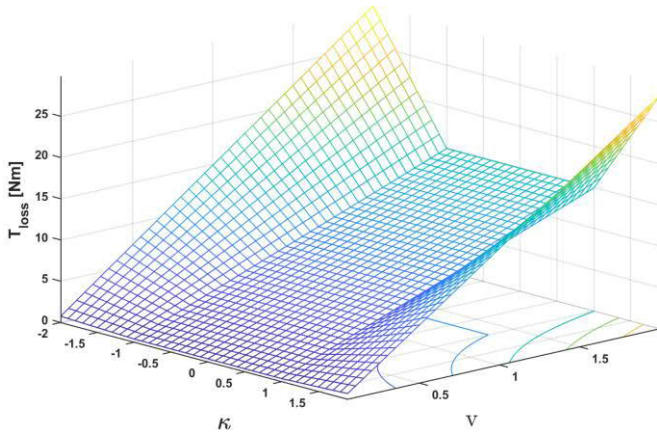


Fig. 7. The effects of κ and velocity on torque loss (mesh).

increased. The shortest path from A to B was along the obstacle with a 90 degree turn at the corner. In the path, the point C_{p4} , describing the distance to the obstacle, was as close to the obstacle edge as possible. By moving C_{p4} further away from the obstacle corner and allowing a larger turning radius, the path becomes longer, but smoother.

Fig. 9 illustrates the five reference paths with different turning radii. The distance to the obstacle edge was increased such that in path 1 the distance is the smallest and in path 5 the largest. The path following errors are illustrated in Fig. 10. Following the shortest path (path 1), the vehicle trajectory deviates from the desired path at the sharp curve and oscillates after it. For the other paths, it can be seen that the path following errors are smaller throughout. Fig. 11 and Fig. 12 illustrate the power demand from the diesel engine for each path. It is evident that with the shortest path, the demand increases temporarily during the turn. Increasing the turning radius reduces the power requirement during the turn up to certain point, after which the turn length starts to increase it. For minimum power consumption, a turning radius can be found between the shortest and the longest path described. During deceleration, the power requirement temporarily becomes negative, as the hydraulic motor acts like a pump and the pump like a motor. Hence, the torque experienced at the pump shaft is negative.

To verify that the dynamics of the HST were the main cause of the path following errors, another set of tests was conducted

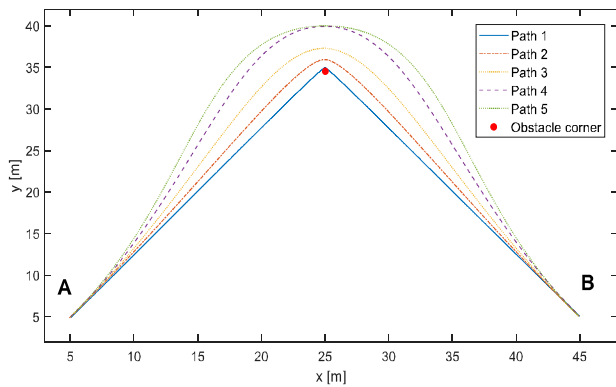


Fig. 9. The reference paths with different turning radii around the obstacle corner.

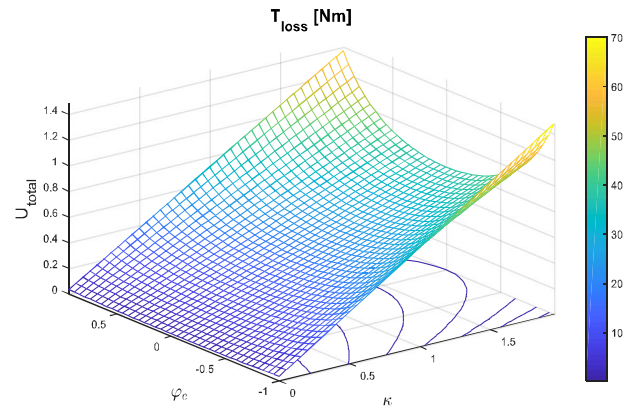


Fig. 8. The effects of control effort U_{total} , heading error φ_e and path curvature κ on torque loss illustrated by the mesh color.

such that the HST dynamics were excluded from the model. The results showed that the overshoot at the tight corner was very small and oscillations hardly occurred. Hence, the effects of the modeled track slipping and the vehicle moment of inertia were smaller than those introduced by the HST.

Based on the illustrated comparisons, it is concluded that sharper turns can decrease the performance of the system. Vehicles with steering, such as car-like or articulated-frame-steerable vehicles, are less concerned about this issue because majority of them have limitations in the steering angle. It is mechanically infeasible to have high curvature driving path or they may become singular at some of these conditions. However, the skid-steer tracked vehicles have no limitation in steering. Based on this study, although the vehicle is capable of rotating on high-curvature pieces of the path, such path properties are not desirable. They will significantly decrease the robot's performance and increase power consumption. A small decrease of κ , for instance increasing radius of a turn, can significantly improve the system performance (as explained for Fig. 8 and Fig. 9) as a compromise of shorter path for better performance and energy efficiency.

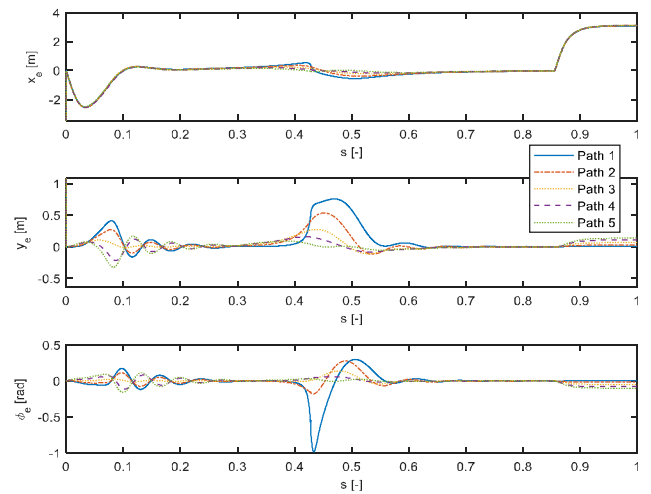


Fig. 10. The heading angle, x- and y-coordinate errors between the desired and actual paths taken by the vehicle.

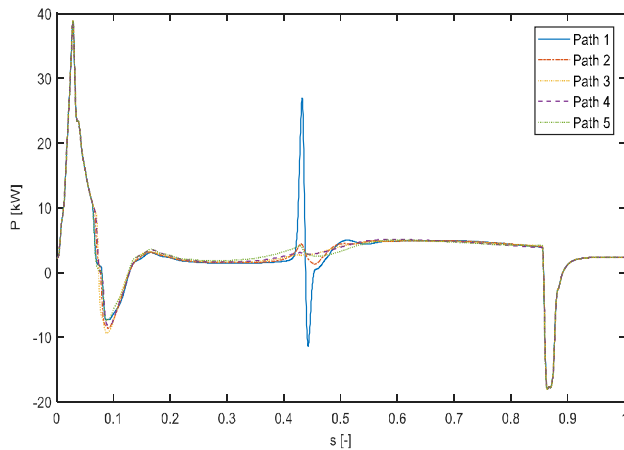


Fig. 11. Power required from the diesel engine during the five test paths. The power temporarily becomes negative during deceleration, as the torque experienced at the pump shaft is negative.

V. CONCLUSIONS

Skid-steering mobile platforms are known for their abilities of heading changes in small spaces. This means no limitation on the minimum rotation radius, as well as boundaries for the path curvature. Considering hydrostatic dynamics in a tracked field robot underlines the lack of optimality in rapid changes of heading in these types of robots. The outcome of this study can be simplified as follows. There are dependencies between the hydro-mechanical losses and geometrical path properties. If the rotation diameter becomes smaller or equal to the vehicle width, the vehicle's dynamics move far from its optimal working points (e.g. path 1 of the tests). Therefore, demand for fast changes in the working point happens more frequently and can be limited by the dynamics of the propulsion. Since, by the formulation proposed in this paper, these losses are shown to be correlated with the path curvature κ , we can conclude that regardless of the velocity or control method, path geometry can decrease the performance of the vehicle at sharp turns.

In terms of path planning criteria, by choosing moderately larger turning radius, about twice the vehicle width (e.g. path 3), power consumption can have smoother changes while the instantaneous center of rotation remains outside of the mobile platform. It can be achieved by considering larger radial margins around obstacles when defining the configuration space for a vehicle, to prevent their instantaneous rotation center from approaching the robot itself. However, too smooth a path will be more demanding, for instance, path 4 and 5 of the tests. The results of this study will be used in future path planning to generate paths for mobile hydraulic machines.

ACKNOWLEDGMENT

This work was funded in part by the Doctoral School of Industry Innovations (DSII) of Tampere University of Technology and the Academy of Finland under project "Autonomous grasping and centralized multimodal human machine interface for multi-site heavy-duty working machines (AUTOGRACE)", grant no. 304604.

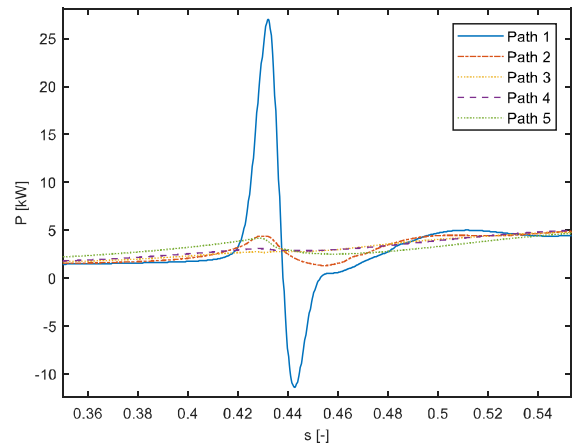


Fig. 12. A segment from Fig. 11 highlighting power consumption during the turn around the obstacle.

REFERENCES

- [1] R. Ghabcheloo, M. Hyvönen, J. Uusisalo, O. Karhu, J. Järä and K. Huhtala, "Autonomous Motion Control of A Wheel Loader," in *ASME 2009 Dynamic Systems and Control Conference*, Hollywood, 2009.
- [2] D. Soetanto, L. Lapierre and A. Pascoal, "Adaptive, Non-Singular Path-Following Control of Dynamic Wheeled Robots," in *The 42nd IEEE International Conference on Decision and Control*, Maui, 2003.
- [3] D. Kim and J. Oh, "Tracking control of a two-wheeled mobile robot using input-output linearization," *Control Engineering Practice*, vol. 7, no. 3, pp. 369-373, 1999.
- [4] R. Oftadeh, M. M. Aref, R. Ghabcheloo and J. Mattila, "Bounded-velocity motion control of four wheel steered mobile robots," in *Advanced Intelligent Mechatronics (AIM), 2013 IEEE/ASME International Conference on*, Wollongong, 2013.
- [5] R. Oftadeh, R. Ghabcheloo and J. Mattila, "Time optimal path following with bounded velocities and accelerations for mobile robots with independently steerable wheels," in *2014 IEEE International Conference on Robotics and Automation (ICRA)*, Hong Kong, 2014.
- [6] J. Fu, F. Tian and T. Chai, "Motion Tracking Control Design for a Class of Nonholonomic Mobile Robot Systems," *IEEE Transactions on Systems, Man, And Cybernetics: Systems*, 2018.
- [7] C. Alfaro, P. Ribeiro and P. Lima, "Smooth Local Path Planning for a Mobile Manipulator," in *Proceedings of Robotica 2004, 4th Portuguese Robotics Festival*, 2004.
- [8] S. Miller, "Simscape Multibody Contact Forces Library," 2017, MATLAB Central File Exchange. [Online]. Available: <https://www.mathworks.com/matlabcentral/fileexchange/47417>. [Accessed 1 March 2018].
- [9] K. Huhtala, "Modeling of Hydrostatic Transmission Steady State, Linear and Non-linear Models," Tampere University of Technology, Dissertations ME 123, 1996.
- [10] M. Hyvönen, J. Vilenius, A. Vuohijoki and K. Huhtala, "Mathematical model of the Valve Controlled Skid Steered Mobile Machine," in *The 2nd International Conference on Computational Methods in Fluid Power, FPN'06*, Aalborg, 2006.
- [11] K. M. Lynch and F. C. Park, *Modern Robotics, Mechanics, Planning and Control*, Cambridge: University Printing House, 2017.